REPORT DOCUMENTATION PAGE

Public reporting burden for this collection of information is estimated to average 1 hour per response, including the time for reviewing instructions, searching existing data sources, gathering and maintaining the data needed, and completing and reviewing the collection of information. Send comments regarding this burden estimate or any other aspect of this collection of information, including suggestions for reducing this burden, to Washington Headquarters Services, Directorate for Information Operations and Reports, 1215 Jefferson Davis Highway, Suite 1204, Arlington, VA 22202-4302, and to the Office of Management and Budget, Paperwork Reduction Project (0704-0188), Washington, DC 20503.

1. AGENCY USE ONLY (Leave blank)	2. REPORT DATE	3. REPORT TYPE AND DATES COVERED
		Final Report 1 June 93 - 31 May 96

4. TITLE AND SUBTITLE
(AASERT-92) Arrays of Efficient Fabry-Perot Modulators for Optical Processing

5. FUNDING NUMBERS

61103D
3484/TS

6. AUTHOR(S)

Professor L. A. Coldren

7. PERFORMING ORGANIZATION NAME(S) AND ADDRESS(ES)
Electrical and Computer Engineering
University of California
Santa Barbara, CA 93106

AFOSR-TR-96

0514

9. SPONSORING/MONITORING AGENCY NAME(S) AND ADDRESS(ES)

AFOSR/NE
110 Duncan Avenue Suite B115
Bolling AFB DC 20332-0001

10. SPONSORING/MONITORING AGENCY REPORT NUMBER

F49620-93-1-0357

11. SUPPLEMENTARY NOTES

19961028 009

12a. DISTRIBUTION/AVAILABILITY STATEMENT

APPROVED FOR PUBLIC RELEASE: DISTRIBUTION UNLIMITED

DISTRIBUTION CODE

13. ABSTRACT (Maximum 200 words)

The goal of this project has been to develop microlenses on the back-side of Vertical-Cavity Lasers (VCLs) and use them in a free-space link. In the process, it was also realized that a simulation program was necessary to evaluate the link. The link simulator program was written in ANSI C, but interfaced with HSPICE, a commercial circuit simulation package, to allow accurate analysis of the laser driver and/or receiver circuit as well as the laser and detector parasitics. Using the program, signals can be traced as they propagate through the link. This not only provides information about the link's performance, but also about link components and their interactions. After describing the program's structure and operation, simulation results will be presented. Two students were involved in this grant. Ms Strzelecka focused on the microlenses and Mr Louderback worked on the link simulator. Ms Strezelecka will be finishing her Ph.D by early 1997 and Mr Louderback is in an earlier stage of his Ph.D work.

14. SUBJECT TERMS

15. NUMBER OF PAGES

16. PRICE CODE

17. SECURITY CLASSIFICATION OF REPORT	18. SECURITY CLASSIFICATION OF THIS PAGE	19. SECURITY CLASSIFICATION OF ABSTRACT	20. LIMITATION OF ABSTRACT
UNCLASSIFSIED	UNCLASSIFIED	UNCLASSIFIED	

NSN 7540-01-280-5500

DTIC QUALITY INSPECTED 1

Arrays of Efficient Fabry-Perot Modulators for
Optical Processing: Microlenses and Link
Simulator for VCSEL Based Links
AFOSR AASERT #F49620-93-1-0357 - FINAL REPORT
6/1/93 - 5/31/96
by
L.A. Coldren: Principal Investigator
D.A. Louderback, E.M. Strzelecka: Students

ECE Technical Report #96-23

Department of Electrical & Computer Engineering

University of California at Santa Barbara

September 30, 1996

Table of Contents

A. Introduction

This report will review the work completed under AFOSR AASERT. The goal of this project has been to develop microlenses on the back-side of Vertical-Cavity Lasers (VCLs) and use them in a free-space link. In the process, it was also realized that a simulation program was necessary to evaluate the link. In this final report we briefly review the microlens work and then focus on detailing the link simulator.

The link simulator program was written in ANSI C, but interfaced with HSPICE, a commercial circuit simulation package, to allow accurate analysis of the laser driver and/or receiver circuit as well as the laser and detector parasitics. Using the program, signals can be traced as they propagate through the link. This not only provides information about the link's performance, but also about link components and their interactions. After describing the program's structure and operation, simulation results will be presented.

Two students were involved in this AASERT - Eva Strzelecka and Duane Louderback. Ms. Strzelecka focused on the microlenses and Mr. Louderback worked on the link simulator. Ms. Strzelecka will be finishing her Ph.D. by early 1997 and Mr. Louderback is in an earlier stage of his Ph.D. work.

B. Micro-Lensed VCSELs

Wafer-level integration of optoelectronic devices with microlenses will result in components that can be used directly in systems, without external optics. Combinations of vertical-cavity surface-emitting lasers (VCSELs), LEDs, or detectors, with microlenses have applications in optical fiber systems, free-space interconnections, displays, printers, etc. Refractive lenses, etched in the back side of the substrate, have several advantages over diffractive lenses. Besides the simple and manufacturable fabrication technology, the lens optical efficiency is primarily limited by the absorption of the substrate, which is nominally transparent. Furthermore, these lenses are far less sensitive to wavelength variations. We present a process for fabricating refractive microlenses in GaAs and InP with the ability to control the radius of curvature (ROC) within ±10%, suitable for many practical applications.

Our microlens fabrication requires transfer of a lens-like shape of patterned, reflowed photoresist[1] into the semiconductor by anisotropic dry etching. We chose reactive ion etching (RIE) over etching with inert ions to achieve faster etch rates and a controllable ratio of the etch rate in the semiconductor to that in the erodable mask material[2]. The latter allows precise control of the lens shape. The lens ROC is primarily controlled by the shape of the mask material. The initial thickness and diameter are of most importance. The initial thickness of the resist is adjusted by controlled etchback in oxygen RIE, after patterning. The semiconductor in the field is etched to form a pedestal, prior to reflow of the resist, in order to create surface tension that prevents the

1

resist from spreading in subsequent reflow, and to preserve the lithographically defined diameter. The polyimide PMGI, used as an erodable mask, forms a nearly-spherical shape after reflow. Finally, the lens shape is transferred to a GaAs substrate in Cl_2 RIE. The final lens shape strongly depends on the ratio of etch rate in the GaAs to that in the PMGI. Two *in-situ* optical monitors in our RIE reactor allow us to control the etch rate ratio thereby achieving a desired curvature and correcting for aberrations. The etch rate of GaAs increases with pressure, due to the increasing chemical nature of the process, whereas the PMGI etch rate remains fairly constant (Fig. B1). The bias voltage proportionately increases the etch rate of both materials. The etch rate of GaAs is about 1.5 to 3 times faster than PMGI. Under typical conditions (2 mT and 350 V bias), the etch rates of GaAs and PMGI are 220, and 110 nm/min, respectively. The initial resist mask is usually thinner than the final GaAs lens, as determined by profilometer scans (Fig. B2). A similar process for InP microlenses in BCl_3/Cl_2 chemistry has been also developed.

For integration with devices, the lens is recessed into the wafer (Fig. B3) for lens surface protection and contact metallization. Integration of GaAs lenses with single mode VCSELs has resulted in reducing the laser's far-field divergence half-angle of ~14° to less than 1.1°.

References to Section B

[1] Z. D. Popovic, R. A. Sprague, and G. A. N. Connel, *Appl. Opt.*, 21, pp. 1281-1284 (1988)
[2] E. M. Strzelecka, G. D. Robinson, M. G. Peters, F. H. Peters, and L. A. Coldren, *Electron. Lett.*, 31, pp. 724-725 (1995)
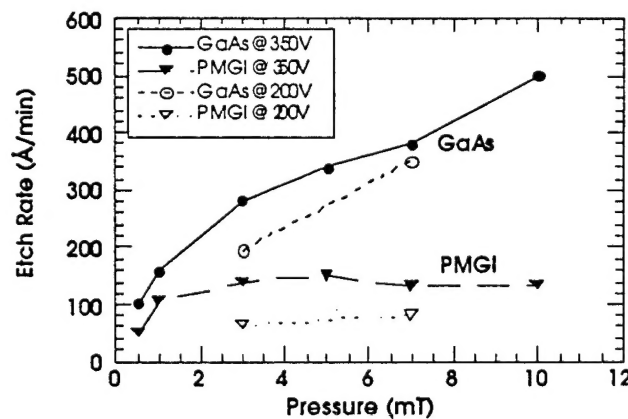
Figure B1. Etch rates of GaAs and PMGI as a function of pressure and bias voltage in CL_2 RIE.
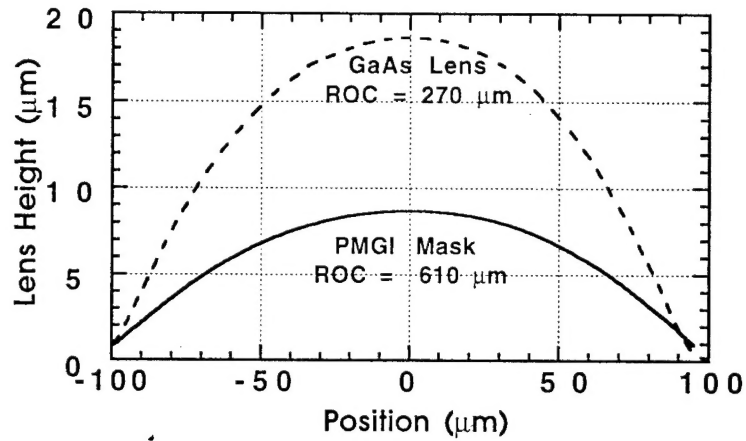
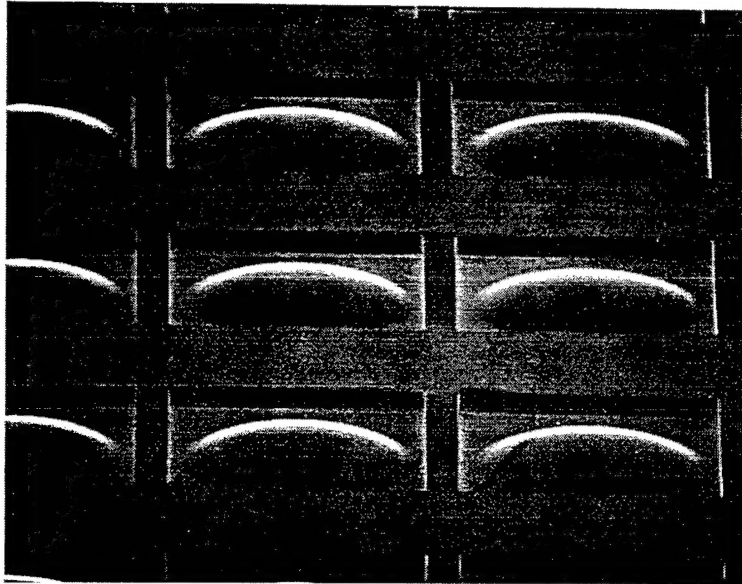Figure B2. Surface profilometer scans of the lens-shaped mask before RIE and the GaAs lens after RIE.

Figure B3. Scanning electron microscope image of a GaAs lens array recessed in the substrate.

C. Link Simulator Program Structure

The basic structure of the link simulator is illustrated in Figure C.1. As the block diagram shows, the program starts by creating a pseudorandom input of current pulses. This current waveform is the input signal to either the laser driver circuit or the laser itself if the circuit is included on the receiver end of the system. This part of the simulation is performed by HSPICE and yields the laser voltage and current waveforms. The laser multimode rate equations are then solved under the constraint of the laser current waveform found previously. The rate equations

3

determine the carrier density, optical power, and chirp waveforms. The program then propagates the signal through either free-space or fiber. For a free-space link, only insertion loss is introduced, but for a fiber link, coupling losses, absorption, and dispersion are included. The detector response, excluding the RC response, is then calculated. HSPICE is invoked to perform the simulation of the RC response of the detector as well as the receiver circuit, if there is one. Finally, the receiver current waveform is filtered. An eye diagram is formed and the results are stored in an output file for graphing.

The pseudorandom pattern generator creates a waveform of supergaussian current pulses and stores it in a file for HSPICE and the subsequent electrical part of the simulation. The pulse magnitude, bit rate, word length, and pulse rise times can be specified by the user in an input file.

If a laser driver circuit is included in the link, an HSPICE description of the circuit is stored in an input file. This input file also contains model files for all devices used in the laser driver circuit. Another input file contains laser parameters including those necessary for an electrical model. The electrical model used for the laser, shown in Figure C.2, is composed of a diode with a resistor, capacitor, and inductor included to account for parasitics. The program combines the laser driver circuit description and laser electrical model into an HSPICE input file. The program then runs HSPICE on the input file and retrieves the resulting laser current and voltage waveforms.
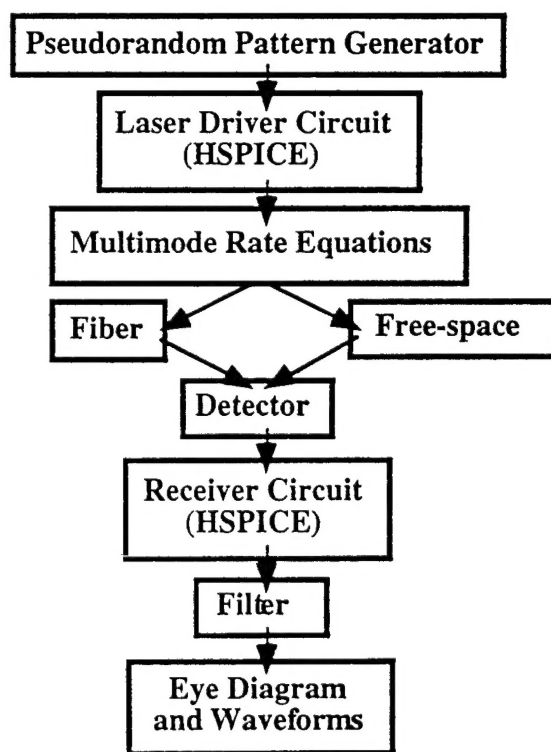

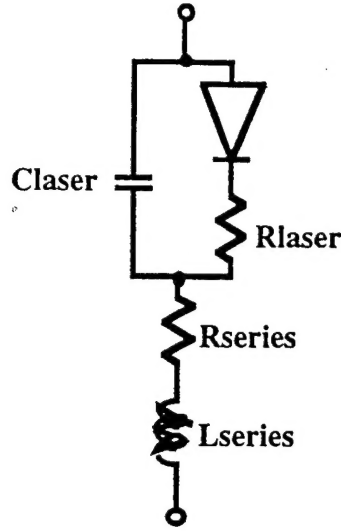Figure C.1: Block diagram of the link simulator.

4

Figure C.2: Electrical model of the laser used in the link simulator.

The laser's multimode rate equations must be solved, consistent with the laser's current waveform, to ascertain the optical power, carrier density, and chirp waveforms. All required laser parameters are contained in an input file. The multimode rate equations are

$$\frac{dN(t)}{dt} = \frac{\eta_i I(t)}{qV} - AN(t) - BN(t)^2 - CN(t)^3 - \sum_m v_{gm} g_m N_{pm}(t)$$

$$\frac{dN_{pm}(t)}{dt} = \left[\Gamma_m v_{gm} g_m - \frac{1}{\tau_{pm}} \right] N_{pm}(t) + \Gamma_m \beta_{sp} BN(t)^2$$

$$\frac{d\phi_m(t)}{dt} = \frac{\alpha}{2} \Gamma_m v_{gm} a \bullet [dN(t)]$$

$$g_m = \frac{1}{\left(1 + \left(\frac{\Delta m}{M} \right)^2 \right)} \bullet \frac{g_o}{1 + \varepsilon N_p(t)} \bullet \ln\left(\frac{N(t) + N_s}{N_{tr} + N_s} \right)$$

where $I(t)$ is the laser current, $N(t)$ is the carrier density, $N_{pm}(t)$ is the photon density in the mth mode, and $\phi_m(t)$ is the phase of the mth mode. $N_p(t)$ is the total photon density summed over all modes. The gain spectrum is approximated by a Lorentzian where m=0 is the mode with the highest gain and M is the mode number where the gain has fallen to half of its peak value [1].

To solve the rate equations, the program begins by calculating the threshold conditions and initial values for the carrier density and photon densities. Then the differential equations are stepped through, point by point, to solve for the variables' values at each point in time. This method of solving these differential equations requires that the time step is very small, on the order

5

of a few ps. Although the number of points can get quite large, the solution of the rate equations only takes a few seconds typically.

Once the optical power and chirp waveforms have been determined, the optical signal must be propagated through either free-space or optical fiber to the photodetector. In the case of a free-space interconnect, the program includes the coupling loss between the laser and detector. In the case of a fiber interconnect, the program includes coupling loss, absorption, and both first and second order dispersion. This produces the optical waveform that will be incident on the photodetector.

The detector response, excluding the RC response, is calculated next. The RC response of the detector is found through HSPICE. Excluding the RC response, the detector's frequency response is

$$\frac{i(\omega)}{i(0)} = \left[\frac{1}{1-e^{-\alpha L}}\right]\left[\frac{1-e^{-j\omega\tau_e}e^{-\alpha L}}{j\omega\tau_e+\alpha L}+e^{-\alpha L}\frac{e^{-j\omega\tau_e}-1}{j\omega\tau_e}+\frac{1-e^{-j\omega\tau_h}}{j\omega\tau_h}+e^{-\alpha L}\frac{1-e^{\alpha L}e^{-j\omega\tau_h}}{\alpha L-j\omega\tau_h}\right]$$

where $\tau_e = L/v_e$ and $\tau_h = L/v_h$. This frequency response is convoluted in the time domain with the detector's dc response, $i(0)=R*P$, to get the detector current without parasitics. The effects of resistance, capacitance, and inductance are ascertained using HSPICE. HSPICE is used for this part of the response because it depends upon the load impedance the detector sees. The load may just be a resistance. However, if a receiver circuit is included, the input impedance of the receiver circuit becomes the load impedance of the detector. This completes the detector response and allows the detector current waveform to be accurately determined.

The program allows a laser driver circuit and/or a receiver circuit to be included in the link. If a receiver circuit is included, HSPICE is used to simulate it at the same time as the RC response of the detector. As with a laser driver circuit, the circuit description is contained in an input file. The program reads the circuit description and creates the appropriate input files for the HSPICE simulation.

Finally, a low pass filter is applied to the receiver output. An eye diagram of the output current is formed by successively shifting and superimposing the output current waveform. The eye diagram and relevant waveforms are stored in output files for graphing and further analysis.

References to section C

[1] L. A. Coldren and S. W. Corzine, *Diode Lasers and Photonic Integrated Circuits*, John Wiley & Sons, Inc., 1995, p. 214-217, 235.

D. Simulations

To demonstrate the operation of the link simulator, it was used to analyze a short distance fiber link using a 980 nm vertical cavity laser (VCL). The VCL had a threshold current of 270 µA and was driven by a three stage common emitter HBT laser driver circuit as shown in Figure D.1. The link also consisted of 2 km of graded index fiber and a small area pin photodetector. A three stage common emitter receiver circuit was used to drive a 50 Ω load and the receiver output was filtered at .7 times the bit rate. The receiver circuit is the same as the laser driver circuit except for the biasing. The waveforms resulting from the link running at 1 Gbit/s are shown in Figures D.2a and D.2b. It can be seen from the waveforms that if the bit rate were increased, pattern dependent effects would begin to appear. Figure D.3 shows eye diagrams of the link's output at 1, 2, 3, and 4 Gbit/s. At the higher bit rates, pattern dependent effects can be seen in the eye diagrams, resulting in eye closure. From the eye diagrams, it appears that this link could probably be operated at up to 3 Gbit/s while still maintaining a low bit error rate.
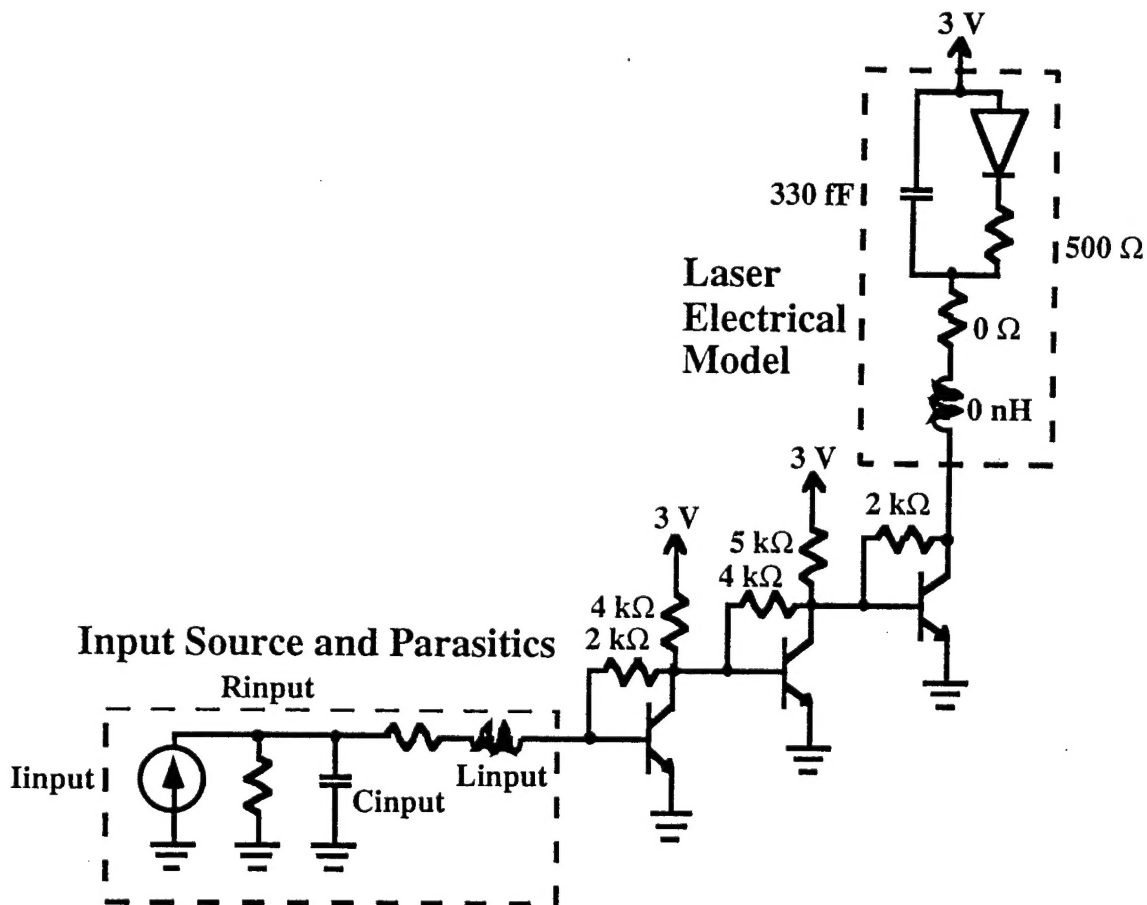

Figure D.1: Three stage common emitter HBT laser driver circuit used in the link simulation. The circuit is used to drive a 270 µA threshold VCL and has a current gain of approximately 20 A/A.
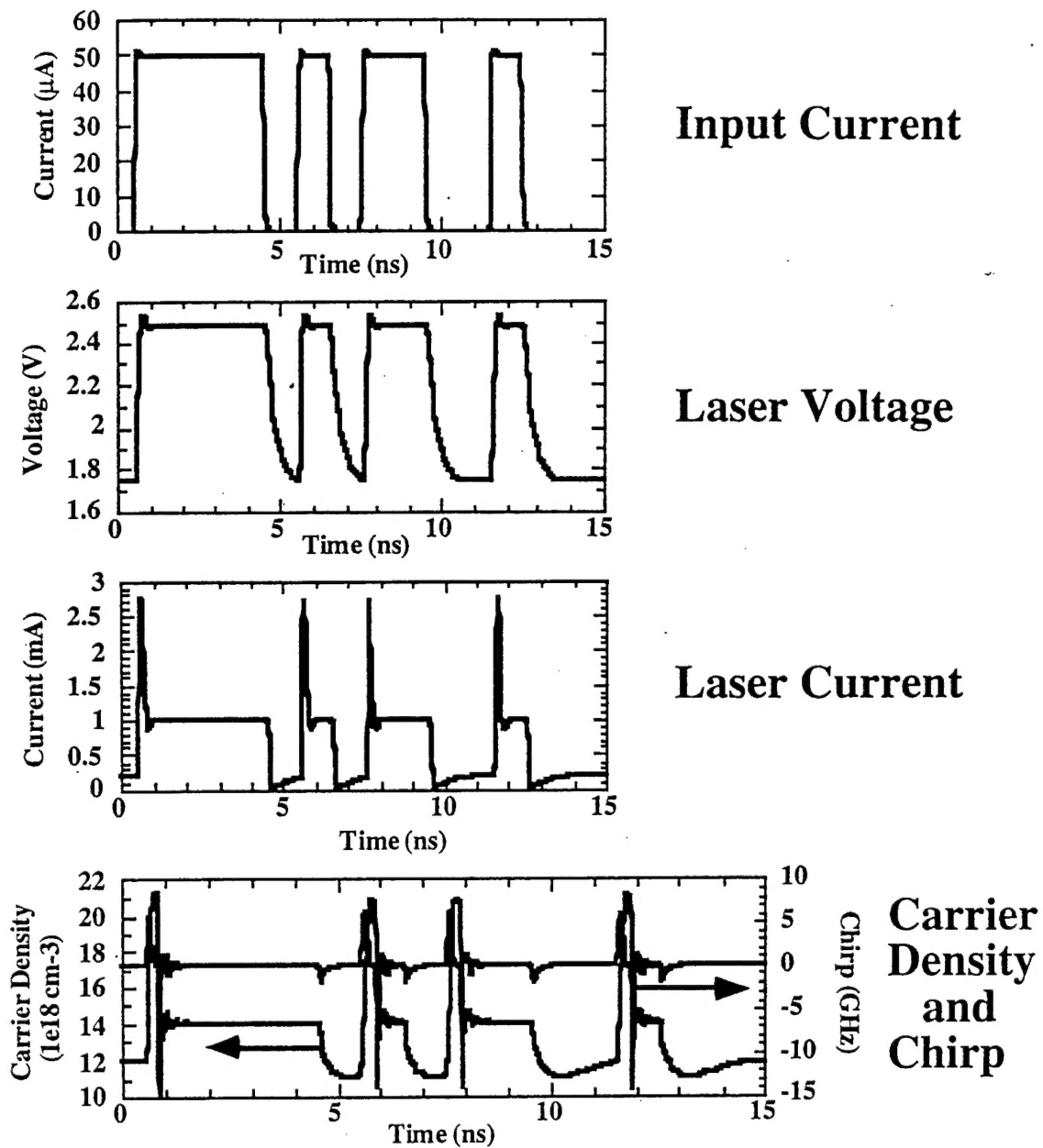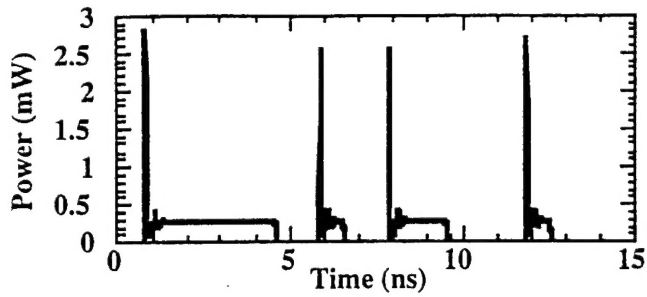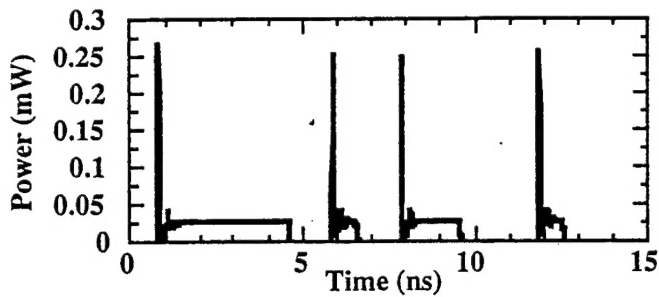
Figure D.2a: Waveforms of the input current, laser current, laser voltage, carrier density, and laser chirp of a fiber link operating at 1 Gbit/s. The link consists of a three stage common emitter HBT laser driver circuit, 270 μA threshold VCL, 2 km of graded index fiber, small area pin photodetector, and receiver filter at .7 times the bit rate.
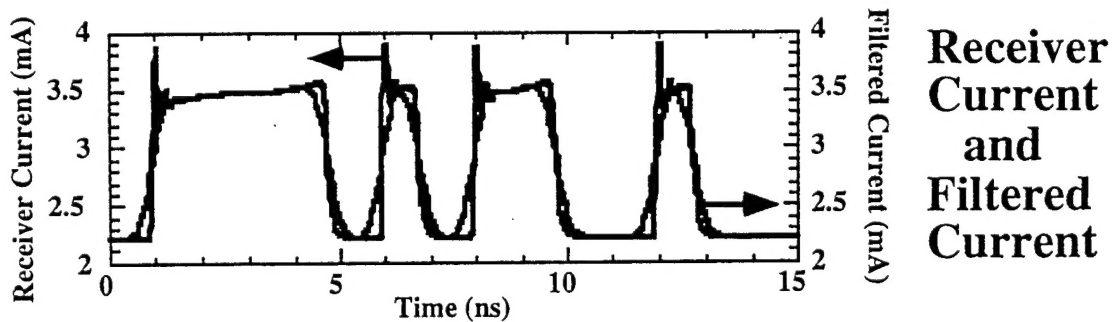
Optical Power Before Fiber

Optical Power After Fiber
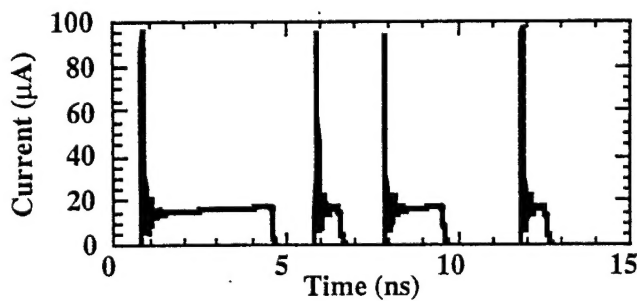
Detector Current

Receiver Current and Filtered Current

Figure D.2b: Waveforms of the optical power before the fiber, optical power after the fiber, detector current, and filtered current of a fiber link operating at 1 Gbit/s. The link consists of a three stage common emitter HBT laser driver circuit, 270 μA threshold VCL, 1 km of graded index fiber, small area pin photodetector, and receiver filter at .7 times the bit rate.
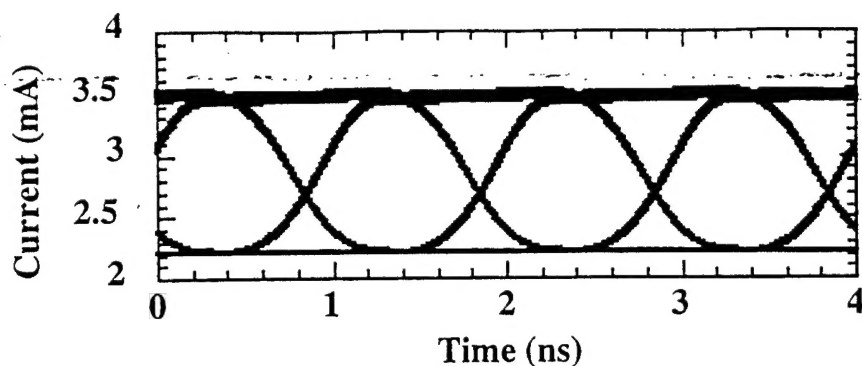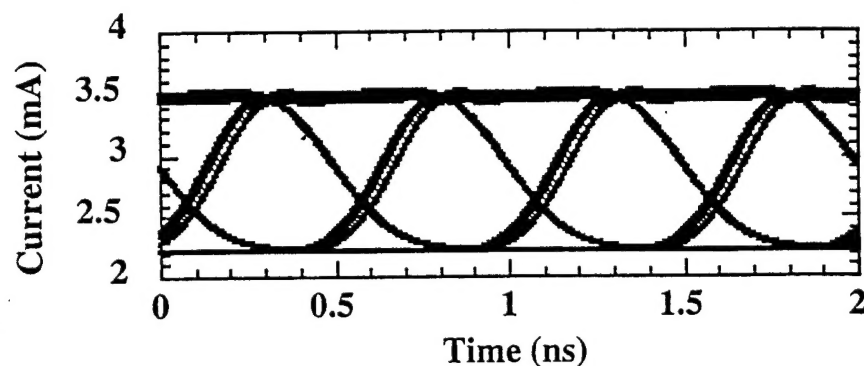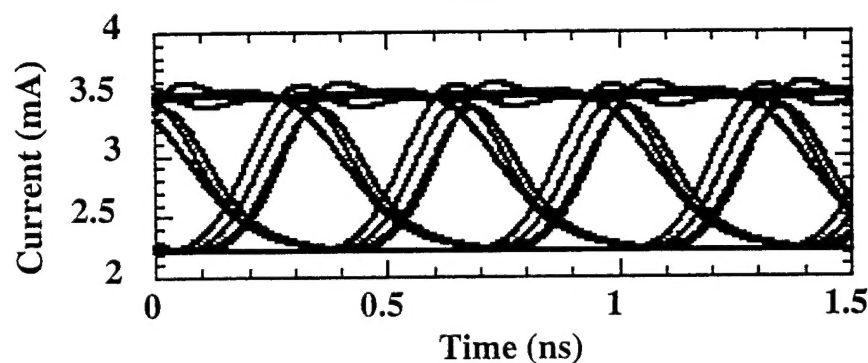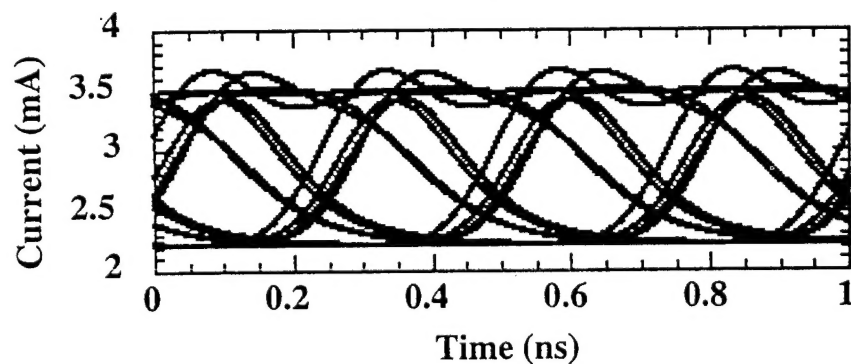
Figure D.3: Eye diagrams of the output at 1, 2, 3, and 4 Gbit/s of a link consisting of three stage common emitter HBT laser driver and receiver circuits, 270 μA threshold VCL, 2 km of graded index fiber, small area pin photodetector, and receiver filter at .7 times the bit rate.

E. List of Publications Partially Supported by AASERT

1 "Integration of Vertical-cavity Laser Diodes with Refractive Microlenses," . E.M. Strzelecka, G.D. Robinson, M.G. Peters, and LA. Coldren, *CLEO '95*, paper no. CWF14, Baltimore, MD, (May 22-26, 1995).

2. "Monolithic Integration of Vertical-Cavity Laser Diodes with Refractive GaAs Microlenses," E.M. Strzelecka, G.D. Robinson, M.G. Peters, F.H. Peters, and L.A. Coldren, *Electronics Letts.*, **31**, (9), 724-725, (April 27, 1995).

3. "Monolithic Integration of Refractive Lenses with Vertical-Cavity Lasers for Optical Interconnections," E. Strzelecka, G.D. Robinson, M.G. Peters, B.J. Thibeault, G. Thompson, L.A. Coldren, *SPIE Photonics West '96*, paper no. 2691-07, San Jose, CA, (January 27 - February 2, 1996).

4. "Multiple-Wavelength MBE-Regrown Vertical-Cavity Laser Arrays Integrated with Refractive Microlenses for Optical Interconnections," E.M. Strzelecka, T. Wipiejewski, J. Ko, B.J. Thibeault, and L.A. Coldren, *15th IEEE Internat'l Semiconductor Laser Conf.*, paper no. P5, Haifa, Israel (October 13-18, 1996).

5. "Monolithic Integration of an Array of Multiple-Wavelength Vertical-Cavity Lasers with a Refractive Microlens for Optical Interconnections," E.M. Strzelecka, T. Wipiejewski, J. Ko, B.J. Thibeault, and L.A. Coldren, *LEOS '96*, paper no. ThA2, Boston, MA, (November 18-21, 1996).

6. "Fabrication of Refractive Microlenses in Semiconductors by Mask Shape Transfer in Reactive Ion Etching," E.M. Strzelecka, G.D. Robinson, L.A. Coldren and E.L. Hu, *MNE '96*, Glasgow, Scotland, (September 23 - 25, 1996).